Supporting Information

for

A New Strategy to Address the Challenges of Nanoparticles in Practical Water Treatment: Mesoporous Nanocomposite Beads via Flash Freezing

Siyuan Pan,[#a] Xiaolin Zhang,[#a, b] Jieshu Qian,[c] Zhenda Lu,[b, d] Ming Hua,[a, b] Cheng Cheng [a] and Bingcai Pan*[a, b]

[a] State Key Laboratory of Pollution Control and Resource Reuse, School of the Environment, Nanjing University, Nanjing 210023, P.R. China.

E-mail: bcpan@nju.edu.cn (B. C. P.) Tel: +86-25-8968-0390

[b] Research Center for Environmental Nanotechnology (ReCENT), Nanjing University, Nanjing 210023, P.R. China.

[c] School of Environmental and Biological Engineering, Nanjing University of Science and Technology, Xiaolingwei 200, Nanjing, 210094, P.R. China.

[d] College of Engineering and Applied Science, Nanjing University, Nanjing 210023, P.R. China

[#] Both authors contributed equally to the manuscript.

This supporting information contains six Figures, i.e., Fig. S1-S7 and supplementary texts.

Supplementary Text

In situ Gran Plots. In situ Gran plots were utilized to determine the equivalence points of potentiometric titration in suspension according to the previous study.[1] The Gran values were calculated according to equation S1 at acidic side or equation S2 at alkaline side:

Acidic side $$G_a = (V_0 + V_{at} + V_b) \times 10^{-pH} \times 10^4 \quad \text{(S1)}$$

Alkaline side $$G_b = (V_0 + V_{at} + V_b) \times 10^{pH-14} \times 10^4 \quad \text{(S2)}$$

Where V_0 represents the initial volume the sample suspension, V_{at} represents the total volume of HNO_3 added in the acidimetric titration, and V_b is the volume of NaOH added in the alkalimetric backtitration. The related equivalence points in the alkalimetric back titrations (V_{eb1} and V_{eb2}) were calculated from the results of linear regression analysis of the Gran plots.[1] At the equivalence point of V_{eb1}, the added titrant is consumed to neutralize the excessive H^+ in solution; while at the equivalence point of V_{eb2}, the added titrant is expected to react with the protonated hydroxyl groups of α-Fe_2O_3 NPs. Based on the Gran plots shown in Fig. S4, we calculated the accessible site density (D_s, mmol g^{-1}) of Fe_2O_3@PS using the PS sample as control according to equation S3:[2]

$$D_s = \frac{(V_{eb2} - V_{eb1})_{sample} \times C_{NaOH} - (V_{eb2} - V_{eb1})_{blank} \times C_{NaOH}}{m_{sample}} \quad \text{(S3)}$$

Where C_{NaOH} represents the concentration of the titrant (mol L^{-1}), m_{sample} represents the dosage of the confined α-Fe_2O_3 NPs (g, in mass of Fe).

Adsorption Kinetic and pH effects. Adsorption kinetics of As(V) by Fe_2O_3@PS is depicted in Fig. S5a. The results indicate that the adsorption rate was significantly enhanced by decreasing the size of the confined α-Fe_2O_3 NPs. The intra-particle diffusion model was employed to represent the kinetic data:[3]

$$Q_t = K_i t^{0.5} + C \quad \text{(S4)}$$

Where Q_t (mg g^{-1}Fe) is the adsorption capacity at time t (h), K_i is the diffusion rate constant (mg g^{-1} $h^{-0.5}$)), and C reflects the relative contribution of initial adsorption and boundary layer diffusion. A linear plot of Q_t vs $t^{0.5}$ means that the adsorption process was controlled by intra-particle diffusion.[3] As shown in Fig. S5b, two of the plots (Rod- and 7nm-Fe_2O_3@PS) are linear and the other (3nm-Fe_2O_3@PS) is multi-linear.

Note that, to clarify the adsorption reactivity of the embedded Fe_2O_3 NPs versus the bare ones, the PS host is inert and hydrophobic, resulting in the equilibrium time required for As(V) adsorption are somewhat long (up to hundreds of hours). To improve the adsorption kinetics of the resultant nanocomposites for real application, we aminated the PS matrix to improve its hydrophilicity prior to hosting 3nm-Fe_2O_3. In detail, during the initial preparation process, the pure PS solution was replaced with the solution containing PS and chloromethylated PS (9:1 in mass) under otherwise identical conditions to that of 3nm-Fe_2O_3@PS. The resultant beads were subject to amination by hexamethylenediamine solution (10%) at 50 ^oC for 6 h, and we obtained a new nanocomposite 3nm-Fe_2O_3@NS. As shown in Fig. S6a, the contact angle of 3nm-Fe_2O_3@NS decreased from 77.0^o of 3nm-Fe_2O_3@PS to 44.7^o, indicating the hydrophilic nature of 3nm-Fe_2O_3@NS. The adsorption kinetics in Fig. S6b described a much faster adsorption rate of As(V) by 3nm-Fe_2O_3@NS, i.e., reaching equilibrium in 24 h.

Effect of pH on As(V) adsorption by Fe_2O_3@PS is elucidated in Fig. S5c. Adsorption of As(V) is highly pH dependent, and the As(V) uptake declined with pH increasing from 4.0 to 8.0. Additionally, the effect of NPs size on As(V) adsorption at a broad pH range (4.0-8.0) is consistent with the order of Q_H values (Fig. 4a-c). Furthermore, the As(V) loaded Fe_2O_3@PS was soaked into 5 wt% NaOH solution to refresh its capacity for cyclic adsorption. Three successive As(V) adsorption- desorption assays indicated that >90% of the loaded As(V) were desorbed from the three nanocomposites (Fig. S7).

Stability of iron-based materials at acidic pHs is of particular concern given the vulnerable properties of iron oxides. The pH-depenent dissolution of Fe_2O_3@PS was determined after incubation for 48 h, and Rod-Fe_2O_3 NPs were employed for comparison. As seen in Fig. S5d, the dissolution of Rod-Fe_2O_3 NPs is significant at pH 1.0-4.0. Since iron oxide dissolution NPs turned more intensive for those of smaller size,[4, 5] the 3 or 7 nm-Fe_2O_3 NPs are believed to be more vulnerable than Rod-Fe_2O_3 NPs. Impressively, the embedded Fe_2O_3 NPs possess enhanced acid resistance over the bare counterparts. It possibly arised from the protection of the polymer host.[6]

References

1. W. X. Liu, Z. X. Sun, W. Forsling, Q. Du and H. X. Tang, *J. Colloid Interf. Sci.*, 1999, **219**, 48-61.
2. C. Tang, J. Zhu, Z. Li, R. Zhu, Q. Zhou, J. Wei, H. He and Q. Tao, *Appl. Surf. Sci.*, 2015, **355**, 1161-1167.
3. J. Wang, S. Zhang, B. Pan, W. Zhang and L. Lv, *J. Hazard. Mater.*, 2011, **198**, 241-246.
4. D. M. Cwiertny, G. J. Hunter, J. M. Pettibone, M. M. Scherer and V. H. Grassian, *J. Phys. Chem. C*, 2009, **113**, 2175-2186.
5. G. Rubasinghege, R. W. Lentz, M. M. Scherer and V. H. Grassian, *P. Natl. Acad. Sci. USA*, 2010, **107**, 6628-6633.
6. B. Pan, H. Qiu, B. Pan, G. Nie, L. Xiao, L. Lv, W. Zhang, Q. Zhang and S. Zheng, *Water Res.*, 2010, **44**, 815-824.

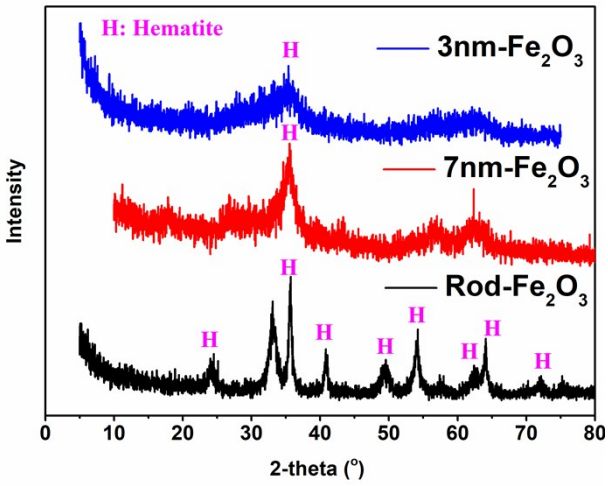

Fig. S1 XRD patterns of the Fe_2O_3 NPs utilized in this study

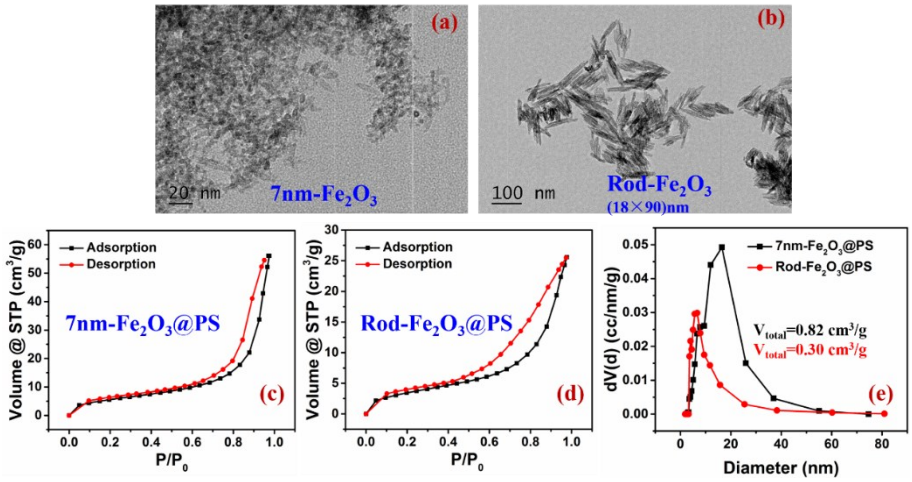

Fig. S2 TEM images of (*a*) 7nm-Fe_2O_3 and (*b*) Rod-Fe_2O_3, N_2 adsorption-desorption isotherms of (*c*) 7nm-Fe_2O_3@PS, (*d*) Rod-Fe_2O_3@PS and (*e*) their pore size distribution based on BJH model.

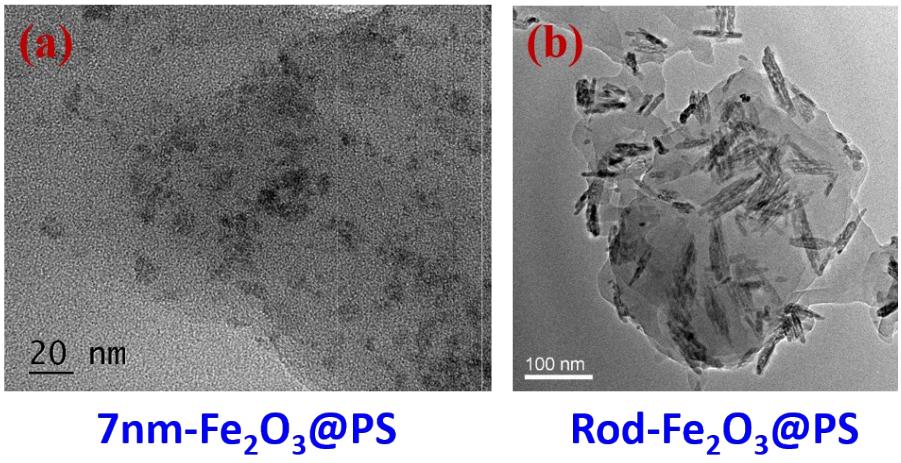

Fig. S3 TEM images of (*a*) 7nm-Fe_2O_3@PS and (*b*) Rod-Fe_2O_3@PS

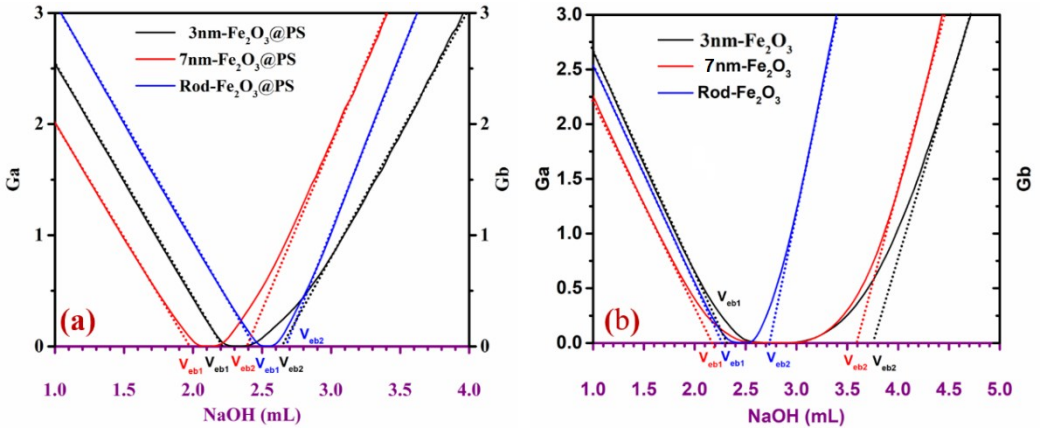

Fig. S4 In situ Gran plots of Fe_2O_3@PS (*a*) and the bare α-Fe_2O_3 NPs (*b*) (Data were collected via potentiometric titration of 0.50 g L^{-1} adsorbent in 0.10 M $NaNO_3$ at 298 K)

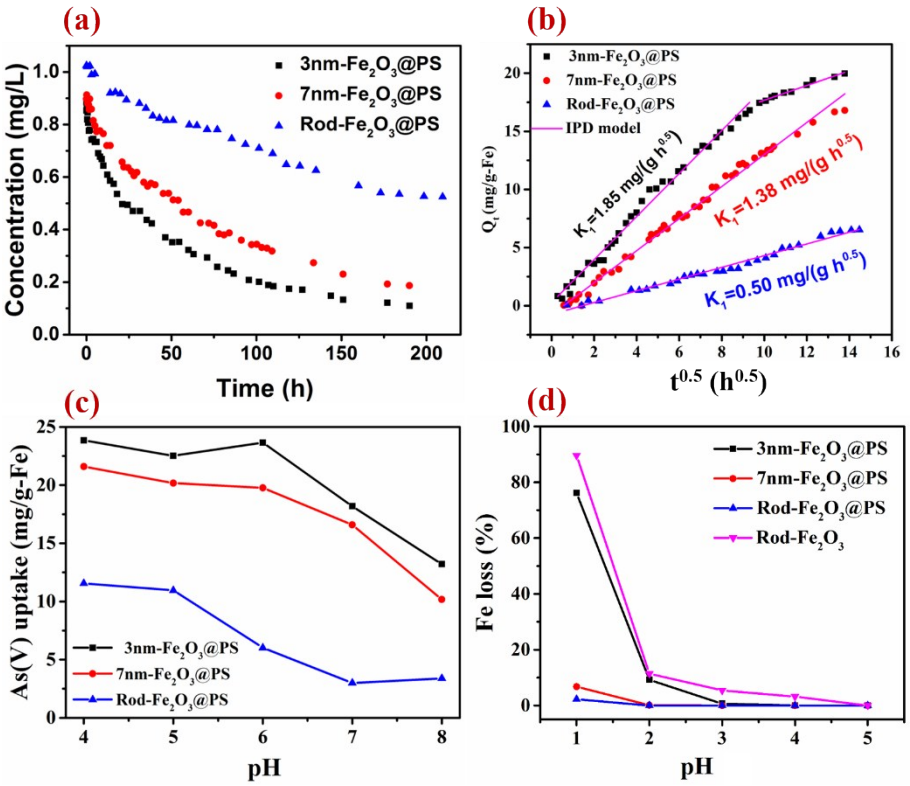

Fig. S5 The adsorption kinetic of As(V) onto Fe_2O_3@PS (*a*), the data fitted by intra-particle diffusion (IPD) model (*b*), effect of pH on As(V) adsorption onto nanocomposite Fe_2O_3@PS (*c*) and the leachate of Fe in 48 h as a function of pH (*d*) (298K, C_0=1.0 mg L^{-1}, dosage=0.50 g L^{-1})

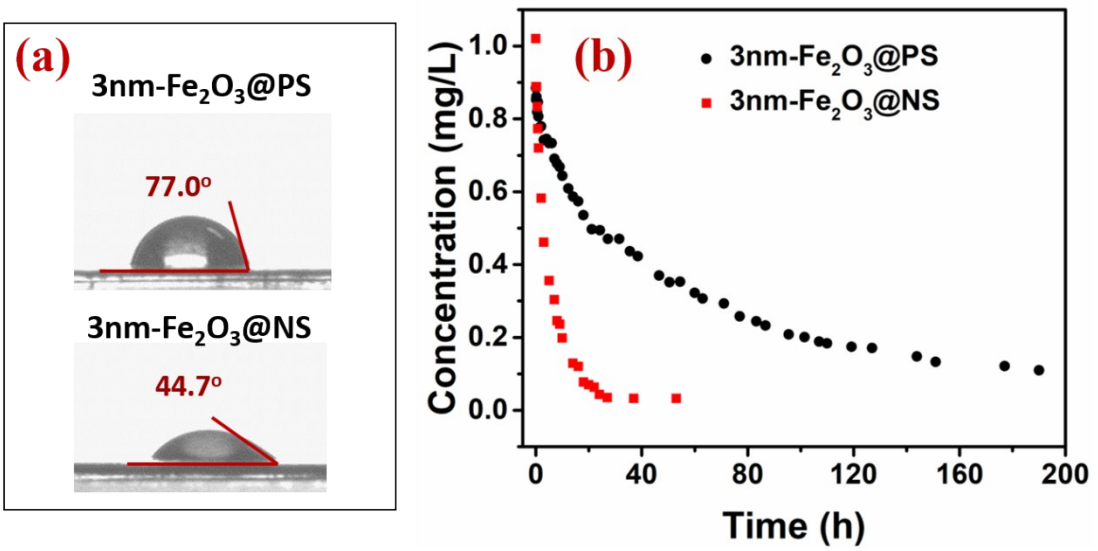

Fig. S6 The contact angle of 3nm-Fe_2O_3@PS and 3nm-Fe_2O_3@NS (*a*), and the adsorption kinetics of As(V) onto 3nm-Fe_2O_3@NS and 3nm-Fe_2O_3@PS (*b*) (298 K, C_0=1.0 mg L^{-1}, dosage=0.50 g L^{-1})

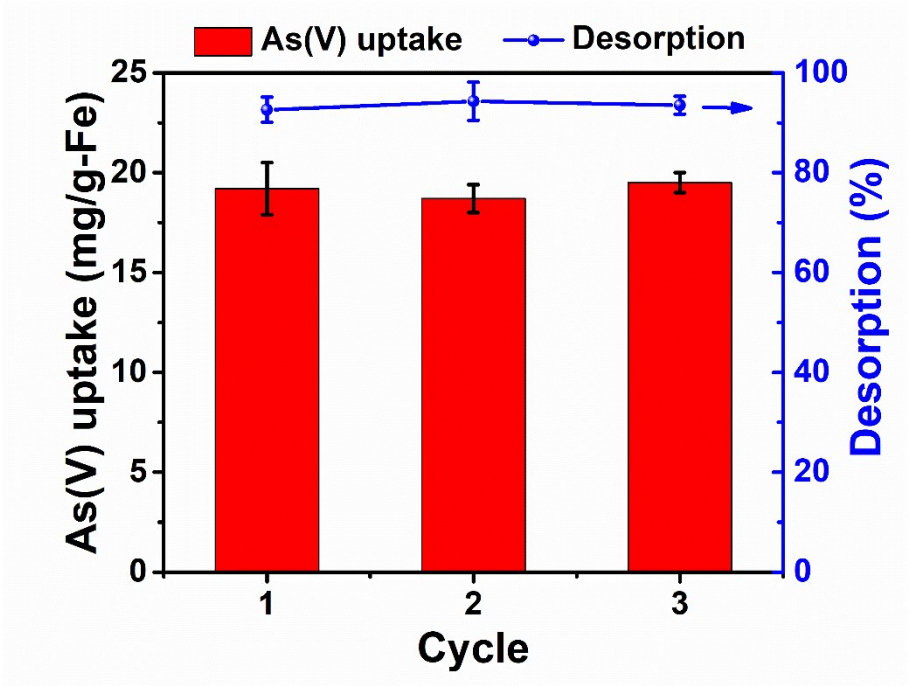

Fig. S7 Cyclic regeneration of the exhausted 3nm-Fe_2O_3@PS in batch mode. (Adsorption condition: 298 K, C_0=1.0 mg L^{-1}, dosage=0.50 g L^{-1}. Regeneration condition: contact with 5 wt% NaOH for 24 h)